fluids

MDPI

Article

The Single Particle Motion of Non-Spherical Particles in Low Reynolds Number Flow

Yuri Mendez

Dynamic Fins Ltd. P. O. Box 74087, RPO Beechwood, Ottawa, ON K1M 2H9, Canada; info@dynamicfinsltd.com or ymendez670@gmail.com; Tel.: +1-613-899-0834

Abstract: This research presents a mathematical framework that places the physics and the dynamics of viscosity within a physical environment that captures the effect of the shape and overall weight of non-spherical particles to calculate their settling velocity. It then takes insights derived from the framework to model analytical constructs to solve the motion of a single particle that settles in a fluid that moves horizontally as a whole. These analytical constructs are then shown to be applicable to spherical and non-spherical particles.

Keywords: non-spherical particle; single particle motion; settling particles; creeping flow; analytical solution

1. Introduction

Consider a 2.65 specific gravity (G_s) spherical particle smaller than 70 micrometers (μm) falling under the action of gravity within a fluid moving at constant horizontal velocity W_x. The particle will be subject to forces exerted by the moving fluid as well as gravity. This motion captures fundamental dynamics that have a profound effect in many fields of science and engineering.

The study of the dynamics of settling particles is still a very active area of research and a tremendous number of original research articles concerning fundamentals, applications, and a multitude of conditions are being published in scientific journals. A set of comparable work could be obtained by applying the following filters:

1. The Reynolds number: the maximum particle Reynolds number calculated on spheres of naturally occurring materials is approximately 0.2. However, the maximum Reynolds number for mineral particles of high aspect ratio (up to 15) can be as high as 2;
2. The problem examined is strictly the fully developed terminal velocity in quiescent fluid;
3. The fluid considered is strictly an incompressible Newtonian fluid without yield stress;
4. When considering infinite dilution, the concentration of solids is not more than about 2% [1] for natural minerals.
5. The problem examined is for solid isolated hard particles without surface roughness;
6. When comparing experimental data, the particle's geometry has been characterized with sufficient detail. Sufficient detail means that accurate particle surface area, dimensions, and overall weight are available in the data set.

The mathematical framework that will be presented in this paper can be considered part of the discussions in the set that fall within the following categories:

(A) Key developments through history;
(B) Recent research: It will be useful to note how active this area of research is today.
(C) Research concerning the physics controlling the terminal velocity of an isolated sphere;
(D) Analytical or semi-analytical studies concerning the terminal settling velocity of non-spherical-particles (NSPs);

check for updates

Citation: Mendez, Y. The Single Particle Motion of Non-Spherical Particles in Low Reynolds Number Flow. *Fluids* **2022**, *7*, 320. https://doi.org/10.3390/fluids7100320

Academic Editors: Sourabh V. Apte and Mehrdad Massoudi

Received: 6 September 2022
Accepted: 27 September 2022
Published: 3 October 2022

Publisher's Note: MDPI stays neutral with regard to jurisdictional claims in published maps and institutional affiliations.

Copyright: © 2022 by the author. Licensee MDPI, Basel, Switzerland. This article is an open access article distributed under the terms and conditions of the Creative Commons Attribution (CC BY) license (https://creativecommons.org/licenses/by/4.0/).

(E) Empirical studies regarding the effect of shape and shape factors;

Key developments (category A) start with Stokes' [2] 1851 solution for flow around a sphere (Stokes' law) as cornerstone development supporting the fundamental assumptions to propose solutions for other geometries and the single particle motion. For particles of spheroidal shape, Overbeck [3] under assumptions along the lines of the Stokes derivation reached a solution for fluid motion around an ellipsoid settling parallel to one of its axes. Ref. [4] later studied the forces acting upon Overbeck's ellipsoid, including the couple (or pair) and the variation of the viscosity as the concentration increases suggested by [5].

In a recent study (category B), Goeree et al. [6] employed Finite Volume and Immersed Boundary Methods to develop a two-dimensional numerical simulation of a free-settling particle in a confined domain to investigate the potential impacts of the surrounding walls on the settling velocity. The settling velocity was found to be lower in comparison with a free settling particle in an infinite domain. Rumin-Caparros et al. [7] conducted a one-year field measurement to study particle fluxes in the Aviles Canyon in the central Cantabrian margin, which is one of the largest submarine canyons in Europe. In this study, total mass fluxes and their major components, such as lithogenics, calcium carbonate, opal, and organic matter, were measured in the settling material. A set of environmental parameters was also measured. Analysis of the data collected in this field campaign explains the sources of particles and the across- and along margin mechanisms involved in their transfer to the deep. Huisman et al. [8] conducted experiments to investigate the settling of heavy spherical particles in a column of quiescent fluid at different Galileo numbers G_a. Settling of both single particles and a swarm of particles were investigated. It was observed that the wake undergoes several transitions for increasing G_a resulting in the particle's successive motions, including vertical, oblique, oblique oscillating, and finally chaotic.

In the formulation and mathematical treatment of the physics controlling the terminal velocity of isolated spheres (category C), there is general agreement on what Hinch [9] simply put as

> "Stokes derived the drag force $6\pi\mu a V$ for an isolated sphere of radius a, moving at velocity, V , through a fluid of viscosity, μ."

The expansion of Stokes' derivation to solve for non-spherical particles or the simpler problem of a cylinder extending to the infinite (Stokes' paradox) is yet to be reached.

The mechanics of the fluid motion around particles of ellipsoidal shape (category D) have later been extended by Breach [10] to include inertial effects. Shi [11] later proposed solutions for spheroids with large aspect ratios. Oseen [12] developed equations to derive a solution for a circular cylinder that is impossible to solve using Stokes' equations (Stokes' paradox). The cylindrical shape has also been the subject of numerous recent articles [13–16]. Other advances to use Stokes' and/or Oseen formulations have been made by Chwang & Wu [17,18].

This study explains an alternative analytical approach that relies on the physics portrayed by viscosity and that can easily be applied to solve Stokes' paradox and non-spherical particles. It also presents a section comparing calculations with the resulting equation and Stokes' law with reference to experimental data sets. The relative differences and the reasons for the deviations are also discussed. Our study fits within the framework of categories C and D.

Along with these advances, there has been a multitude of research papers proposing empirical correlations (category E), shape factors, and, more recently, fractals [19–22] to address other geometries. Dharmarajah [23], in completing a study to develop an empirical model to predict the expansion of fluidized non-spherical particles, examined fundamental questions regarding settling velocities and shape factors based on settling velocities. Dharmarajah examines numerous correlations to the effect of particle shape within the framework of drag theory. Drag theory will generally involve the calculation of a frontal area that represents the magnitude of the drag for a given shape. Johnstone et al. and Heywood [24,25] provided arguments to support that the calculation of the frontal area should be based on the diameter of the projected area, while [26–28] provided arguments to support that the frontal area calculated from the projected area of a sphere of equivalent volume is a preferred approach. Others have sought to find relationships involving Reynolds number and other forms of shape factors such as sphericity [27,28] or other measures of particle dimensions [25,29,30].

In spite of the research effort briefly over-viewed above, Silva et al. [31] note regarding settling suspensions:

> "their inherent complexity has yet to be properly predicted by a unified numerical model or empirical correlation."

This article proposes an examination of the potential of this mathematical framework to reduce the burden of this deficiency. The framework is unified in a coherent analytical connection between the physics controlling the terminal settling velocity of spheres to the physics controlling the settling velocity of non-spherical particles and the transport mechanisms for any particle shape with relatively minimal assumptions.

2. Fundamentals

The following is a known outcome of the viscous flow between flat plates separated by a distance $2Y$ driven by a pressure gradient ∇P (Poiseuille flow) to compute the shear stress τ at any height y between the flat plates measured from the center line between the plates:

$$\mu \frac{du}{dy} = \tau_w \frac{y}{Y} \tag{1}$$

where τ_w is the wall shear at the surface of the plate and y and Y have units of distance or length. It should be noted that y and Y are tributary volumes m^3 of fluid per square meter m^2 of the surface where the fluid is tributary to (m^3/m^2). For flat surfaces y distance in m is the same quantity as y (m^3/m^2) but not for spheres. For free settling spherical particles driven by gravity g, the τ_w at the wall of the solid particle of radius r_s having a density of ρ_s within a fluid of density ρ_f is known and can be simply seen as the submerged weight of particle per square meter of particle and calculated as

$$\tau_w = \frac{r_s}{3}(\rho_s - \rho_f)g \tag{2}$$

The spherical volume of the ambient fluid that is "tributary" per square meter of particle h (comparable with y in Equation (1)) can be computed at any distance r within the ambient fluid of radius R as

$$h = \frac{\frac{4\pi r^3}{3} - \frac{4\pi R^3}{3}}{4\pi r^2} = \frac{r^3 - R^3}{3r^2} \tag{3}$$

and the maximum spherical tributary volume H can be computed as $(r_s^3 - R^3)/(3r_s^2)$. Figure 1 (comparable with Y in Equation (1)) presents the environment that is captured with this relationship which leads to the following expression to compute the shear stress over any distance r within the ambient fluid:

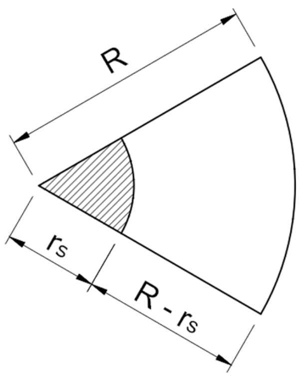

Figure 1. Spherical tributary volume.

$$\mu\frac{du}{dy} = \frac{-\tau_w}{(\frac{r_s^3-R^3}{3r_s^2})}(\frac{r^3-R^3}{3r^2}) \tag{4}$$

Equation (4) can then be integrated and find the following expression for the settling velocity profile along the ambient spherical tributary volume:

$$u = \frac{-\tau_w}{2\mu(\frac{r_s^3-R^3}{3r_s^2})}(\frac{r^2}{3} + \frac{2R^3}{3r} - R^2) \tag{5}$$

At the wall of the solid sphere $u = V_s$ and $r = r_s$. Hence:

$$V_s = \frac{-\tau_w}{2\mu(\frac{r_s^3-R^3}{3r_s^2})}(\frac{r_s^2}{3} + \frac{2R^3}{3r_s} - R^2) \tag{6}$$

and matching V_s with the experimental data R is found. Equations (4)–(6) imply the existence of a pressure gradient ∇P_f that affects the motion of free settling particles because

$$\frac{\tau_w}{(\frac{r_s^3-R^3}{3r_s^2})} = \nabla P_f \tag{7}$$

∇P_f is also found. Note that Equation (7) computes the same value of ∇P_f for any particle size in a given fluid and temperature. As $\nabla P_f h = \tau$ and $\tau = \mu$ where the velocity gradient $((\mathrm{m/s})/\mathrm{m} = \mathrm{s}^{-1})$ equal to 1, the tributary volume h_1 where the velocity gradient equal to 1 and $\tau = \mu$ can also be computed as $h_1 = \mu/\nabla P_f$ from the experimental results and Equation (7) leading the way to write the following expression for ∇P_f:

$$\nabla P_f = \frac{\mu}{h_1} \tag{8}$$

Bearing in mind that h_1 is in $\mathrm{m}^3/\mathrm{m}^2$ one can convert h_1 to $\mathrm{kg/m}^2$ per unit velocity gradient θ as $\theta = h_1\rho_f$ (in $(\mathrm{kg}-\mathrm{s})/\mathrm{m}^2$) and re-write Equation (8) as

$$\nabla P_f = \frac{\mu\rho_f}{\theta} \tag{9}$$

with θ calculated as $1.148 \times 10^{-3}(\mathrm{kg}-\mathrm{s})/\mathrm{m}^2$ at different temperatures in water and subjected to further validation in water, Cyclohexane and Toluene [32].

As we have discovered a way to compute ∇P_f from Equation (9), R is available from Equation (7) to then substitute ∇P_f and R in Equations (5) and (6) to compute the velocity profile from $r = r_s$ to $r = R$ and/or the boundary value V_s on the wall of the solid sphere. Hence Equation (5) takes the form of

$$u = \frac{P_f}{2\mu}(\frac{r^2}{3} + \frac{2R^3}{3r} - R^2) \tag{10}$$

and Equation (6) takes the form

$$V_s = \frac{P_f}{2\mu}(\frac{r_s^2}{3} + \frac{2R^3}{3r_s} - R^2) \tag{11}$$

This can all be simplified by noting that $\nabla P_f h$ computes τ, meaning that the volume of fluid will expand in proportion to the stress via h and that the stress itself mobilized by the particle is higher in proportion to the submerged weight of the particle. Thus, one can establish these volumetric proportions by dividing the volume of fluid "trapped" in ambient expansion by the volume of the solid sphere, further referred to as the maximum tributary ratio e_{max}. The term maximum is necessary because the same ratio can be established for any shear stress surface within the ambient fluid. This volumetric relationship can, thus, be written as

$$e_{max} = \frac{4/3\pi R^3 - 4/3\pi r_s^3}{4/3\pi r_s^3} = \frac{R^3 - r_s^3}{r_s^3} \tag{12}$$

Hence:

$$R = r_s(1 + e_{max})^{1/3} \tag{13}$$

and

$$R - r_s = r_s((1 + e_{max})^{1/3} - 1) \tag{14}$$

leading to the equation below

$$V_s = \frac{\nabla P_f r_s^2}{2\mu}(1 + \frac{2e_{max}}{3} - (1 + e_{max})^{2/3}) \tag{15}$$

to achieve the same as Equation (6) when Equation (13) is substituted into Equation (6).

As ∇P_f multiplied by the volume of the entire ambient ambient expansion computes the submerged weight of the particle, it should be noted that

$$4/3\pi r_s^3(\rho_s - \rho_f)g = \nabla P_f(4/3\pi r_s^3(1 + e_{max}) - 4/3\pi r_s^3) \tag{16}$$

or

$$e_{max} = \frac{(\rho_s - \rho_f)g}{\nabla P_f} \tag{17}$$

which further makes Equation (15) to compute V_s on the wall of the solid sphere very simple.

From the volumetric relationship established by e and because the driving stress is proportional to the submerged weight per square meter of the solid particle, it can be seen and verified that the volume of fluid per square meter of the particle is $e_{max} r_s/3$ so that

$$e_{max}\frac{r_s}{3}\nabla P_f = \tau_w \tag{18}$$

A close look at the $\frac{r^3 - R^3}{3r^2}$ mathematical expression in Equation (4) is noteworthy. It computes the tributary volume h overlying any spherical surface within the ambient expansion of fluid and it accomplishes this on account of the geometry and size of the entire system. It is this expression that affords all the flexibilities to analyze, examine, and model simple dynamics for the free settling velocity of non-spherical particles, cylinders, "flatter surfaces" and hindered settling velocity of particles of any shape, as will be seen later in this article.

Another fact that is noteworthy is that in reaching any value of velocity using Equation (15), the entire mechanics leading to the value rely on the working mechanics in Equation (5). It includes a proper account of the required amount of ambient pressure gradient required to mobilize τ_w and the computation of the velocity profile through the tributary volume in the per square meter basis that accounts for the entire size of the system.

2.1. Non-Spherical Particles

From Equation (2), it can be seen that τ_w is the submerged weight of the volume of the particle B_{nsp} per square meter A_{nsp} of the particle for any particle shape as

$$\tau_w = \left(\frac{B_{nsp}}{A_{nsp}}\right)(\rho_s - \rho_f)g \tag{19}$$

and from all the equations presented leading to the velocity, the characterizations are per square meter of the particle (or per unit area). Simply put, the equations leading to the velocity of NSPs rely on the construction of a pseudo-sphere (or equivalent sphere) of radius $r_{s,eq}$ whose total area and wall shear are the same as the NSP. Hence,

$$r_{s,eq} = \left(\frac{A_{nsp}}{4\pi}\right)^{1/2} \tag{20}$$

The wall shear of the non-spherical particle τ_{nsp} is captured by the construction of the ambient fluid capable of mobilizing τ_{nsp} and bearing the required relationship with the entire ambient fluid. This ambient fluid will, thus, have the same volume as the volume "retained" in the ambient fluid of the NSP. Given the constructions leading to $r_{s,eq}$, the new volumetric relationship $e_{max,eq}$ need to be established for the particle of $r_{s,eq}$ radius mobilizing τ_{nsp}. For an NSP of volume B_{nsp}, the new volumetric relationship can be seen to take the form:

$$e_{max,eq} = \frac{e_{max} B_{nsp}}{4/3\pi r_{s,eq}^3} \tag{21}$$

where e_{max} is as established by Equation (17) for the specific gravity of the NSP. τ_{nsp} can be verified to be computed from the new volumetric relationship as

$$\tau_{nsp} = \frac{r_{s,eq}}{3} e_{max,eq} \nabla P_f \tag{22}$$

to verify that the construction meets the equilibrium requirements. The boundary value of the velocity V_{nsp} at the wall of the non-spherical particle (NSP) can hence be established from Equation (15) written as

$$V_{nsp} = \frac{\nabla P_f r_{s,eq}^2}{2\mu}\left(1 + \frac{2e_{max,eq}}{3} - (1 + e_{max,eq})^{2/3}\right) \tag{23}$$

2.1.1. Validation and Exemplary Application for Non-Spherical Particles

As in science and engineering, there is a great interest in modeling the settling velocity of naturally occurring materials such as clay minerals, a euhedral pseudo hexagonal plate of Georgia Kaoline clay (kGa-1) is presented here as a non-spherical case to demonstrate the implementation of the proposed model for such cases.

As explained above, the driving stress τ_w can be the same for different particle shapes and have different velocities. As they have the same driving stress, they also have the same tributary volume but different curvatures, as shown in Figure 2 presenting the geometry with dimensions in microns of two tributary volumes mobilizing the same τ_w. The calculations leading to the dimensions shown Figure 2 are described later in this section. In Figure 2, the spherical region of radius R represents the proxy construct leading to the velocity profile and velocity on the wall of the kGa-1 particle and the smaller spherical region represents a sphere that mobilizes the same wall shear as kGa-1. The quantity $R - r_{s,eq}$ = 0.786 in Figure 2 from the volumetric relationships is

$$R - r_{s,eq} = r_s((1 + e_{max,eq})^{1/3} - 1) \tag{24}$$

for the NSP and from Equation (14) for spheres. Although this is a specific case study, the same rules presented here apply to any other non-spherical particle.

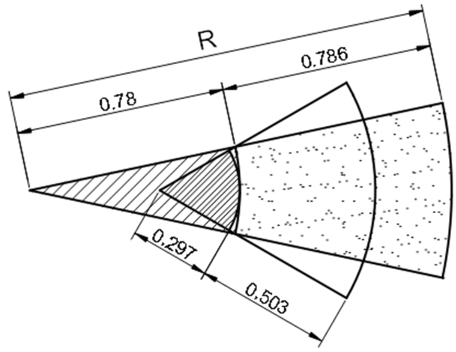

Figure 2. Tributary volumes of the same magnitude and different shapes (microns).

Zbik & Smart [33] measured settling velocity of 0.44 micrometers ($\mu - m$) per second (s) for the median particle size of Georgia Kaolinite (KGa-1). KGa-1 is a known source clay for which the median particle size (length dimension) has been measured to be in the order of $2\mu - m$ (and this length is just close) and 4 to 10 aspect ratios [33,34]. To represent this median particle size consider an euhedral pseudo hexagonal plate of Georgia Kaolinite clay with a specific gravity of G_s = 2.65, thickness of $T = 0.25\mu - m$, aspect ratio (α) of $\alpha = 8.65$ and edge length (or radius) of $a = 1.08\mu - m$ (the length (or diameter enclosing the hexagon) is, thus, 2.16 μm) settling in water at 20 °C. The surface area A of this non-spherical particle can be calculated as $A = 3\sqrt{3}a^2 + 6aT = 7.70 \times 10^{-12}$ m^2 and the volume B is $B = 3\sqrt{3}a^2T/2 = 7.6 \times 10^{-19}$ m^3. The submerged weight of this particle is $M_s = (\rho_s - \rho_f)B_{nsp}g = 1.23 \times 10^{-14}N$, therefore, its wall shear stress is 0.0016 N/m^2 as computed from Equation (19). The radius of a spherical particle of the same density with a wall shear stress equal to the wall shear stress of this non-spherical particle is $r_s = 0.297\mu - m$ (Equation (2) and Figure 2). Although this spherical particle with radius $r_s = 0.297\mu - m$ has the same wall shear stress and driving stress as that of the Georgia Kaoline clay particle considered here, it settles at a different velocity due to its different geometry (and smaller overall weight). One can now apply the construction in Equation (20) to build a flatter (or having lower curvature) velocity profile and also apply the construction in Equation (21) to build the size of the ambient fluid that will mobilize the given τ_w and that will mobilize the submerged weight of the particle when applied throughout the surface area of the particle to compute the settling velocity of the non-spherical Georgia Kaoline clay (and the entire velocity profile if needed) as

$$V_s = -\frac{\nabla P \times r_{s,eq}^2}{2\mu}\left[1 + \frac{2e_{max,eq}}{3} - (1 + e_{max,eq})^{2/3}\right], \quad (25)$$

where $r_{s,eq}$ is the equivalent radius defined as the radius of a sphere with a surface area and τ_w equal to the surface area and τ_w of the non-spherical particle. For the specific case presented here $r_{s,eq} = 0.78$μm from Equation (20). Note also that $e_{max,eq}$ in Equation (25) can be seen to be the volume of the bulk fluid region around the non-spherical particle divided by the volume of the equivalent spherical particle as $e_{max,eq} = B \times e_{max}/(\frac{4}{3}\pi r_{s,eq}^3)$ as expressed in Equation (21). This construction ensures that the wall shear mobilized on the surface of the equivalent sphere will be equal to the wall shear of the non-spherical kGa-1 (which can be verified via Equation (22)) and that this wall shear will develop across the ambient fluid having less curvature to represent the non-spherical shape (whose velocity profile can be computed from Equation (10)). In the case discussed here, $e_{max,eq}$ can be calculated as $e_{max,eq} = 7.6 \times 10^{-19} \times 18.57/(\frac{4}{3}\pi(0.78 \times 10^{-3})) = 7.1$. $R - r_{s,eq}$ is, thus, $0.786\mu - m$ and $R - r_s = 0.503\mu - m$ for the sphere with the same τ_w and h as shown in Figure 2. Note the substantial difference in geometry for the same amount of fluid per square meter of particle. The velocity profile is, thus, computed through a thicker tributary volume for the NSP leading to a greater value of velocity.

By substituting $r_{s,eq} = 0.78$ μm and $e_{max,eq} = 7.1$ in Equation (25), the settling velocity of the euhedral pseudo hexagonal plate of Georgia Kaoline clay in water at 20 °C is found to be

$V_s = 0.446 \times 10^{-6}$ m/s. Note how well it compares with the $V_s = 0.44 \times 10^{-6}$ m/s measured by Zbick & Smart [33] for the median particle size having very similar dimensions. The 0.297 µm radius particle at 20 °C settles at $V_s = 0.233 \times 10^{-6}$ m/s, which is calculated to show that a spherical particle having the same wall shear and tributary volume as the non-spherical particle settles slower than the non-spherical and heavier KGa-1 particle. This construction takes away any ambiguity in the definition of the effect of particle shape.

The mathematical constructions leading to Equation (25) ensure that the driving shear stress and the fluid response on the equivalent sphere are of the same magnitude as the non-spherical Kaoline computed through a velocity profile and tributary volume that are flatter (or have less curvature $1/r$) than a sphere that has the same τ_w. As mentioned above, Equations (10) and (25) calculate the value of the velocity on the wall of the solid sphere; however, the entire velocity profile can be obtained for any condition. Additional validation of this model for non-spherical particles is presented in [32].

2.2. Stokes' Paradox

The following is a solution for the settling velocity u of a cylinder of infinite length [16] using the analog mathematical constructs derived under this model:

$$u = -\frac{P_f}{2\mu}\left(\frac{r^2}{2} + R_c^2 ln\left(\frac{R_c}{r}\right) - \frac{R_c^2}{2}\right) \tag{26}$$

which can be solved from the surface of the cylinder where $r = r_c$ to $r = R_c$ where the velocity is 0. R_c can be found from

$$R_c = r_c(1 + e_{max})^{1/2} \tag{27}$$

The settling velocity of the cylinder V_{sc} is calculated by making $r = r_c$ in Equation (26) or from the volumetric relationships as

$$V_{sc} = \frac{\nabla P_f r_{sc}^2}{4\mu}(ln(1 + e_{max}) + e_{max} ln(1 + e_{max}) - e_{max}) \tag{28}$$

3. Comparison with Stokes' Law

Stokes' law is accepted as a relationship that has great merits and accuracy in depicting the processes leading to the equilibrium velocity of settling particles, so that almost every piece of research for more than 160 years in this field is "benchmarked" in Stokes' law. Although the formulation explained above does not move along the assumptions made by Stokes, it departs from the same origin: the momentum equation. A check by benchmarking the results with reference to Stokes' law is necessary and beneficial to the discussion in connection with the challenges explained in the introduction. Stokes' law is presented below.

$$V_o = \frac{2(\rho_s - \rho_f) r_s^2 g}{9\mu} \tag{29}$$

In contrast, the end result of this formulation is the velocity profile from Equation (5), which further evolves into Equation (6) for the boundary value of V_s on the wall of the solid sphere pasted below for ease of reference.

$$V_s = \frac{\nabla P_f}{2\mu}\left(\frac{r_s^2}{3} + \frac{2R^3}{3r_s} - R^2\right) \tag{30}$$

which can also be written as Equation (15) also pasted below for ease of reference

$$V_s = \frac{\nabla P_f r_s^2}{2\mu}\left(1 + \frac{2e_{max}}{3} - (1 + e_{max})^{2/3}\right) \tag{31}$$

in which the factor between brackets will be quoted as the maximum expansion ξ_{max}. It is called expansion because it expands and contracts with temperature and varies in size with the specific gravity of solids within a given fluid.

To examine the applicability of these relationships, the data sets in [35–37] reproduced by Cheng [38], who measured the settling velocity of naturally occurring particles of spherical shape and ρ_s of 2650 kg/m^3 at 15 °C shows that the deviations from the experimental data become visible in particles of 61 µm diameter. Assuming that the limit occurs at a point just below this particle size, or 55 µm, the limit can be defined as a velocity gradient $du/dr = \tau_w/\mu$ of approximately 155 s^{-1} which corresponds to a Reynolds number of 0.25 (as computed from Stokes' relationship) and from this evidence this limit appears accurate. The velocity gradient appears to be a good rational means to define this limit as knowledge of the velocity is not required a priori.

Although the assumptions made to reach Equation (30) are different from those made under Stokes' mathematical formulation, the results of both relationships are not too different. Generally, at 20 °C Equation (30) delivers a velocity that is about 30% lower than Stokes' law for the same particle size and the variation of the velocity with temperature is slightly more than Stokes' law.

To put these relationships in context with some experimental data, it is important to bear in mind the following limitations and challenges:

1. A comprehensive review of the literature on the subject indicates that experimental results in which the geometry of the particles is characterized with sufficient accuracy and detail are rare.
2. Weatherly [1] has shown that for naturally occurring minerals, the concentration limit at which particles can be considered to behave as a single particle is approximately 1.9% volume fraction. This limit filters out many articles.
3. As outlined for the range of sizes in the colloidal range in Wang et al. [39], "Despite the fact that there exist several techniques capable of characterizing nanoparticle sizes, their measurement results from the same sample often deviate from each other by an amount that is considered significant on the nanometer scale", so there is additional uncertainty on the actual particle sizes.
4. Velocity fluctuations: Mucha et al. [40] developed a flow model for these fluctuations and discusses "the discord and debate about what sets the size of these fluctuations". They find that "These discrepancies are substantial enough to suggest that there is another effect in the experiments that goes beyond the physics heretofore included in the simulations" and they discuss other suspected effects; however, we argue that Mucha et al. and the literature, in general, miss an effect that may be very important and mentioned in Mendez [32]: seismic ambient noise and air noise. Seismic ambient noise consists of permanent ground vibrations originating from natural and anthropogenic sources at any location. Seismic noise is often in the range of a few microns to 10 microns but amplitudes from anthropogenic sources up to a few hundred microns are not rare. Intuition indicates that where displacement amplitudes are easily a factor of 20 greater than the length of the particles themselves, there is a strong case for their influence on velocity fluctuations.

Due to the scale problem in 4 and as a result of practical experience in signal processing, the following is hypothesized:

(i) most experimental results are greatly influenced by seismic and air noise (and other factors discussed in the literature), particularly in the lower portion of the particle size range (the colloidal range) and
(ii) that the net effect is expected to be an increase in the velocity so that measured settling velocities are higher than they would otherwise be in quiescent fluid.

A recent study [41] using a noninvasive technique measured the settling velocity of latex particles and the results were compared with the Stokes relationship in which they noted that particles in the higher range of sizes settled slower than those predicted by

Stokes and in close agreement with the lower range of particle sizes. This is in agreement with data reproduced in Table 2 in [32] from [35–37,42] reproduced by Cheng [38] in the higher particle size range in which Stokes' relationship computes a velocity that is greater than observed and Equation (11) is in better agreement with the data and also data from Table 2 [32] within the colloidal range from [43,44] in which Stokes' law is in better agreement with the experimental data in contrast with Equation (11) which computes a velocity that is less than observed. These data sets lead to the following regarding the results obtained from Equation (11) and Stokes' law: *In the higher portion of particle sizes above the colloidal range Equation (11) computes a velocity in better agreement with the experimental data, and in the lower range of particle sizes, the Stokes relationship is in better agreement*. Here it is argued that measurements in the colloidal range are highly influenced by seismic noise and other effects outlined in the literature. The net effect of seismic noise is a greater velocity than what the particles would otherwise have in quiescent fluid, so if properly accounted for, Equation (11) may well be in better agreement with the experimental data throughout the entire range of particle sizes.

Advantages of Using Equation (11)

Most of what there is to say regarding the accuracy of these two relationships are outlined in the last paragraph of the previous section. Most research has sought to capture the physics within the framework of the mathematical formulation of Stokes' law to apply them to other geometries. To that end, some progress has been made in analytical studies; however, the end result in the majority of cases is some form of scaling law to the end result of the formulation for spheres. This also applies to empirical studies and the hindered regime included. The literature, the experimental evidence, and the framework presented in this article strongly suggest that the approach with a scaling law is reasonably justified. Hence, the corollary to the body of research is that the physics and the scaling laws are not yet well understood. In a fundamental sense, the framework presented in this article is distinct in that it provides means to capture the natural scaling laws within the physics and the dynamics of viscosity to solve the settling velocity of particles. The framework, thus, has revealed fundamental insights to remove much of the ambiguity regarding the effect of particle size, shape, and overall weight of particles. These insights have been conducive to a coherent easy path to solve difficult geometries such as solutions for non-spherical particles, Stokes' paradox, and aggregates [32,45,46] which have been subject to validations with sedimentation experiments [33,34,47] conducted in hexagonal Kaoline (kGa1) having mean measured lengths in the order of $2\mu - m$ and aspect ratios in the order of 4 to 10 and also highly non-spherical flaky plates of mica having aspect ratios exceeding 10 and thicknesses in the order of 6 to 8 μm producing a close match to the experimental data.

The constructs noted above may seem overly simplistic; however, a close examination exposes numerous deep insights. One of those insights is that the concept of curvature $(1/r)$ is not explicitly or at least not deliberately implemented in the relationships. One can hence use the term "flatter" to describe an object having a curvature relatively lower than another and model its effect. Another insight is that although not explicitly shown in the final relationship, the τ_w is the driving stress which removes much of the ambiguity in representing the effect of the particle size, shape, and overall weight. And yet another insight is the construct between brackets in Equation (4) which computes cubic meters that "tribute" per square meter of the surface within the ambient fluid, which subsequently decreases (thus having greater curvature) as it approaches the solid sphere. However, another insight is that it takes a certain amount of ambient fluid to mobilize a given wall shear and that this ambient fluid will have a different physical dimension depending on the curvature of the particle and yet that the entire ambient fluid with a given geometry will be capable overall to mobilize the submerged weight of the particle. It is, thus, an ideal averaging physical construct to represent non-spherical geometries.

The end goal of these constructs for given driving stress is the construction of a velocity profile across a volume of fluid capable of mobilizing the required shear stress and having the constitutive relationship of curvature that represents the geometry and the overall submerged weight of the given particle. These very basic concepts and simple constructs accomplish many of the goals sought in the literature in this field and have afforded great flexibility to address non-spherical particles of any shape and aggregates. Thus, we can engineer reasoned solutions to other problems, such as the single particle of any shape motion, as shown in the following sections.

4. The Relaxation Time

From the stand of equilibrium and basic physics, the processes controlling the attenuation (or increase) of the velocity difference between the solid particle and the fluid are fundamental to the particle motion and so are recognized in the literature. The relationship:

$$t_{st} = \frac{2(\rho_s - \rho_f)r_s^2}{9\mu} \tag{32}$$

is accepted to compute the time that it takes for a free settling particle to reach its terminal velocity (relaxation time) t_{st}. It does not take an in-depth examination of it to see that t_{st} is the time that it would take a particle to reach the velocity computed by Stokes' law as if it was falling in a vacuum with no resistance under an acceleration equal to g. While one can throw this t_{st} to a physicist and tell him that this is the best approximation available, it is an insult to try to have him accept it as true and to look no further to a better answer. An insult that this author is not willing to accept with a number of rejections in "scientific" journals.

It is basic physics that if one applies a force to an object, it accelerates at a rate in proportion to the force per kilogram mass of the object in $\mathrm{m/s^2}$. If at a time t_1 the force is x and at a later time t_2 the force is y and greater than x, the acceleration is greater at time t_2 so that the acceleration a is not constant. Where one is provided with the means to compute the force at any time t, the varying acceleration is available, and the relaxation time can be computed as explained below.

Consider a variable acceleration changing at a given rate ω $(\mathrm{m/s^3})$. Acceleration a at time t is, thus, ωt and the average acceleration a at time t is, thus, $\frac{\omega t}{2}$. Integration of the acceleration with respect to time t produces the velocity at time t as $V = \frac{\omega t^2}{4}$. In this context, the relaxation time will be defined in simple terms as the time lag required to build up the bulk-fluid region with an effective radius of R_{eff} around the particle. Note that Equation (11) can be used to calculate the velocity u' of the particle (velocity at wall) when the bulk fluid region around the particle is growing and the equilibrium condition has not been reached (i.e., at any time during the time lag to achieve equilibrium). Hence,

$$u' = \frac{\omega t^2}{4} = -\frac{\nabla P \times r_s^2}{2\mu}\xi \tag{33}$$

where $\xi = [1 + \dfrac{2e}{3} - (1+e)^{2/3}]$. At time $t = T$ the terminal velocity V_s is reached so that $u' = V_s$, $e = e_{max}$ and $\xi = \xi_{max}$. Note that u' is distinct from u in Equation (10). u is the velocity at any point in a fully developed velocity profile where the velocity profile exists up to R, whereas u' is the velocity on the wall of the sphere at time t within a profile whose maximum extent is defined by $e < e_{emax}$. In other words, it is R that is changing in Equation (11) to preserve the goal of obtaining the velocity of a particle at time t within the context of the relaxation time.

Within the context of Equation (18) at time $t, e < e_{max}$ so that $(r_s/3)e\nabla P$ expresses the force per square meter of particle exerted from the fluid and $[(r_s/3)(\rho_s - \rho_f)]$ expresses the submerged mass of the particle in kilograms per square meter of particle. At any time t, the force per kilogram of the particle (or acceleration) from the forces delivered by the fluid to the particle is

$$a = \frac{(r_s/3)e\nabla P}{[(r_s/3)(\rho_s - \rho_f)]} = \frac{e\nabla P}{\rho_s - \rho_f} \tag{34}$$

As $a = \omega t$, one can write

$$\omega t = \frac{e\nabla P}{\rho_s - \rho_f} \tag{35}$$

to calculate the acceleration at time t, where $0 < t < T$. The relaxation time occurs at equilibrium, when $t = T$, $e = e_{max}$, and $\xi = \xi_{max}$. With that, combining Equations (33) and (35) yields,

$$T = \frac{2r_s^2\xi_{max}(\rho_s - \rho_f)}{\mu e_{max}} \tag{36}$$

This is to say that the relaxation time at 20 °C is about three times more than predicted by Equation (32).

The Relaxation Time of Non-Spherical Particles

It can be seen from Equation (34) that for a non-spherical particle the relationship turns into

$$a = \frac{(r_{s,eq}/3)e\nabla P}{[(B_{nsp}/A_{nsp})(\rho_s - \rho_f)]} \tag{37}$$

and the relaxation time is

$$T = \frac{6r_{s,eq}^2\xi_{max,eq}(\rho_s - \rho_f)(B_{nsp}/A_{nsp})}{\mu e_{max,eq}} \tag{38}$$

The concepts studied for the construction of solutions for non-spherical particles were used to derive a solution for the relaxation time of non-spherical particles, which is one of the main goals of this paper.

5. The Single Particle Motion

Consider a particle of density ρ_s subject to gravity g within a fluid of density $\rho_f < \rho_s$ who is moving horizontally at velocity W_x. The fluid reacts to the imbalance induced by the particle via shear stress that adds up via the mechanics of viscosity to a resulting wall shear τ_w. τ_w is the vector sum of the shear stress force caused by gravity in the vertical (y) direction indicated by τ_{wy} and the shear stress force induced by the moving fluid in the horizontal x direction denoted τ_{wx}. τ_{wy} can be seen to take the form $\tau_{wy} = \tau_w cos(\beta)$, where β is the angle between the total resulting shear stress τ_w and a vertical line. The vector problem can hence be solved on a two-dimensional plane and the problem of finding the velocity of the particle V_x relative to the velocity of the flow W_x is reduced to finding τ_{wx}. Although the relationships and the underlying mechanics presented in this section are simple, the resulting horizontal component of the driving stress is not intuitively apparent. Note that in this problem, there is no horizontal body force acting on the particle, and the horizontal component of the force is caused by hydrodynamic processes.

The only aspects that are apparent are that: (1) a larger bulk fluid region around the particle will be affected by the motion of the particle due to the greater force induced by the addition of the horizontal flow force component and (2) from a physics standpoint, the particle will never move at the same velocity as the fluid (W_x), due to its greater inertia. It slides and moves slower.

Assessment of this condition via basic inertial considerations let us realize that for the fluid, the particle is only a concentration of mass. Hence, if we ignore gravity, the particle is able to induce an imbalance in the fluid by virtue of its mass difference. From the standpoint of the dynamics portrayed in the introduction, as the fluid responds only to the imbalance induced by the mass of the particle, the pressure gradient caused by the particle motion will be effective over a bulk fluid region with a mass equal to the submerged mass of the particle. Therefore, the volume of fluid $V_{b.f.r}$ that will influenced by the particle will have mass $\rho_w G_f V_{b.f.r}$ equal to the mass difference between the particle of volume V_s mass $G_s \rho_w V_s$ and the fluid's mass $G_f \rho_w V_s$ that it displaces. This can be written as

$$\overbrace{G_s\rho_w V_s - G_f\rho_w V_s}^{Submerged\ mass\ of\ particle} = \overbrace{\rho_w G_f V_{b.f.r}}^{Mass\ of\ bulk\ fluid\ region\ response}, \tag{39}$$

The volumetric relationship $\dfrac{V_{b.f.r}}{V_s}$ is also be established as

$$e_{max,h} = \frac{V_{b.f.r}}{V_s} = \frac{G_s}{G_f} - 1 = \frac{\rho_s - \rho_f}{\rho_f} \tag{40}$$

$e_{max,h}$ is the ratio of the bulk fluid region around the particle through which the pressure gradient and the shear stress caused by the horizontal motion of the particle are effectively divided by the volume of the particle. It is worth noting that similar to $e_{max,v}$, i.e., the ratio of the volume of the fluid region affected by the vertical motion of the particle under gravity, $e_{max,h}$ is totally independent of the size of the particle and depends only on the density of the particle and fluid properties. For instance, the volume of the bulk fluid region affected by the *horizontal* motion of a particle with a specific gravity of 2.65 is 1.65 times the volume of the particle, i.e., $e_{max,h}$ = 1.65. Note that the actual bulk fluid region affected by particle motion is larger than that and this value only represents the impact of *horizontal* motion and does not include the effect of vertical motion due to gravity.

Because we know the volume of the fluid affected by the particle due to the horizontal velocity, we also know the force that will be mobilized against the particle as $e_{max,h} \times V_s \times \nabla P$ is the force in Newtons so that the acceleration a_x is

$$a_x = \frac{e_{max,h} \times V_s \times \nabla P}{(\rho_s - \rho_f)V_s} = \frac{e_{max,h} \times \nabla P}{(\rho_s - \rho_f)} = \frac{\nabla P}{\rho_f} \tag{41}$$

The acceleration $a_{x,y}$ that affects the particle can, thus, be found as

$$a_{xy} = \sqrt{g^2 + a_x^2} \tag{42}$$

The maximum tributary ratio e_{max} for this condition establishes the volume of the bulk fluid region around the particle that is affected by the pressure gradient created in response to both the *vertical* and *horizontal* components of the motion. The total e_{max} can be calculated using Equation (17), where g is substituted for the total acceleration a_{xy} as

$$e_{max} = \frac{\rho_s - \rho_f}{|\nabla P|} a_{xy} \tag{43}$$

in which a_{xy} is defined as

$$a_{xy} = \sqrt{g^2 + a_x^2} \tag{44}$$

The e_{max} calculated via Equation (43) is then substituted into Equation (10) to calculate V_{xy}, which is the total velocity of the particle. The horizontal component of the total velocity of the particle is then calculated as

$$V_x = V_{xy} sin\beta \tag{45}$$

where $\beta = tan^{-1}(\dfrac{a_x}{g})$.

This velocity is, of course, relative to the velocity of the flow W_x. So, for a viewer in a fixed position, the observed horizontal velocity is $V'_x = W_x - V_x$. The total velocity of the particle is then $V' = \sqrt{V'^2_x + V_y^2}$ making an angle of $\beta' = tan^{-1}(\frac{V'_x}{V_y})$ with the vertical.

Exemplary Single Particle Motion for a Natural Highly Non-Spherical Particle

For a solid particle moving at water at 20 °C, $a_x = \frac{\mu}{\phi} = 0.8737 \frac{\text{N}}{\text{kg}}$ so that the acceleration of the particle is $a = \sqrt{a_x^2 + g^2} = 9.846$ N/kg, assuming $g = 9.807$ N/kg at an angle of $\beta = 5.091°$ with the vertical. Using Equation (43), $e_{max} = 18.65$, i.e., the volume of the bulk fluid region affected by the horizontal and vertical motions of the particle is 18.65 times the volume of the particle itself, which is just slightly larger than the volume of the bulk fluid region affected by the particle in the case of a purely vertical motion, for which e_{max} was found to be 18.57, to mobilize the additional acceleration caused by the horizontal motion. The resulting V_{xy} velocity for the KGa-1 particle presented in Section 2.1 can, thus, be computed as follows: the volume of fluid retained in the expansion is $18.65 \times 7.6 \times 10^{-19}$ m^3 equal to 1.419×10^{-17} m^3. The radius of a sphere having the same area as the KGa-1 particle is $r_{s,eq} = 0.783$ µm, leading to an $e_{max,eq}$ of 7.063, as explained in Section 2.1 By substituting these values into Equation (23), the total velocity of the particle is calculated as 4.55×10^{-7} (which was found to be 4.46×10^{-7} in Section 2.1 for pure vertical motion), with a horizontal component of 0.404×10^{-7}. If one assumes that the KGa-1 particle is subject to a horizontal velocity of $W_x = 1$ mm/s, the particle will have a velocity of $W_x - V_x = 9.9996 \times 10^{-4}$ m/s at an angle of 89.986 degrees with respect to the vertical (i.e., almost horizontal) in the view of a stationary observer. The outcome is not intuitively unexpected, as we see very heavy objects drifting with very little resistance in currents. Note that the nature of equilibrium in fluids renders the condition of fluid motion characterized by a single horizontal value nearly impossible, except perhaps in the open ocean. Thus, even at very low velocities, precipitation of small solids will not occur.

Funding: This research was funded by its author.

Data Availability Statement: Not applicable.

Acknowledgments: I would like to thank Kevin Slattery Bouchey, P. E. and Ahmadreza Vasel-Be-Hagh, Mechanical Engineering Department of the Tennessee Technological University for the feedback provided during the production of this article.

Conflicts of Interest: The author declares no conflict of interest.

Abbreviations

The following abbreviations are used in this manuscript:

MDPI	Multidisciplinary Digital Publishing Institute
DOAJ	Directory of open access journals
TLA	Three letter acronym
LD	Linear dichroism

References

1. Weatherly, W.C. The Hydrometer Method for Determining the Grain Size Distribution Curve of Soils. Master of Science Thesis, Department of Civil Engineering, Massachusetts Institute of Technology, Cambridge, MA, USA, 1929.
2. Stokes, G.G. On the effect of the internal friction of fluids on the motion of pendulums. *Camb. Philosofical Soc.* **1851**, *9*, 8–106.
3. Oberbeck, A. Ueber stationare flussigkeitsbewegung mit berucksichtigung der inneren reibung. (On steady state fluid flow and the calculation of the drag.). *J. Reine Angew. Math.* **1876**, *81*, 62–80.
4. Jeffery, G.B. The motion of ellipsoidal particles immersed in a viscous fluid. *Proc. R. Soc. Lond. Ser. A Contain. Pap. Math. Phys. Character* **1922**, *102*, 161–179.
5. Einstein, A. A new determination of molecular dimensions. *Ann. Phys.* **1906**, *324*, 289–306. [CrossRef]
6. Goeree, J.; Keetels, G.; van Rhee, C. Particle settling using the Immersed Boundary Method. In Proceedings of the 18th International Conference on Transport and Sedimentation of Solid Particles, Prague, Czech Republic, 11–15 September 2017; Matousek, V., Sobota, J., Vlasak, P., Eds.; Wroclaw University of Environmental and Life Sciences: Wroclaw, Poland, 2017; pp. 81–88.
7. Rumin-Caparros, A.; Sanchez-Vidal, A.; Gonzalez-Pola, C.; Lastras, G.; Calafat, A.; Canals, M. Particle fluxes and their drivers in the Aviles submarine canyon and adjacent slope, central Cantabrian margin, Bay of Biscay. *Prog. Oceanogr.* **2016**, *144*, 39–61. [CrossRef]
8. Huisman, S.G.; Barois, T.; Bourgoin, M.; Chouippe, A.; Doychev, T.; Huck, P.; Morales, C.E.B.; Uhlmann, M.; Volk, R. Columnar structure formation of a dilute suspension of settling spherical particles in a quiescent fluid. *Phys. Rev. Fluids* **2016**, *1*, 074204. [CrossRef]

9. Hinch, J. A perspective of Batchelor's research in micro-hydrodynamics. *J. Fluid Mech.* **2010**, *663*, 8–17. [CrossRef]
10. Breach, D.R. Slow flow past ellipsoids of revolution. *J. Fluid Mech.* **1961**, *10*, 306–314. [CrossRef]
11. Shi, Y. Low Reynolds numbers flow past an ellipsoid of revolution of large aspect ratio. *J. Fluid Mech.* **1965**, *23*, 657–671. [CrossRef]
12. Oseen, C.W. Stokes' formula and a related theorem in hydrodynamics. *Arkiv. Mat. Astron. Fysik* **1910**, *6*, 20.
13. Monson, D.R. The Effect of Transverse Curvature on the Drag and Vortex Shedding of Elongated Bluff Bodies at Low Reynolds Number. *J. Fluids Eng.* **1983**, *105*, 308–318. [CrossRef]
14. Jordan, S.A. Spatial Resolution of the Axisymmetric Turbulent Statistics Along Thin Circular Cylinders at High Transverse Curvatures and Low-Re. *J. Fluids Eng.* **2012**, *134*, 091206. [CrossRef]
15. Champmartin, S.; Ambari, A.; Richou, A.B. Kinematics of a Cylindrical Particle at Low Reynolds Numbers in Asymmetrical Conditions. *J. Appl. Fluid Mech.* **2019**, *12*, 1629–1640. [CrossRef]
16. Mendez, Y. A Flow Model for the Settling Velocities of Non Spherical Particles in Creeping Motion. Part III. Slender Bodies, the Stream Functions, the Flow and the Momentum Equation. *J. Appl. Fluid Mech.* **2015**, *8* , 391–398. [CrossRef]
17. Chwang, A.T.; Wu, T.Y. Hydromechanics of low-Reynolds-number flow. Part 1. Rotation of axisymmetric prolate bodies. *J. Fluid Mech.* **1974**, *63*, 607–622. [CrossRef]
18. Chwang, A.T.; Wu, T.Y.T. Hydromechanics of low-Reynolds-number flow. Part 2. Singularity method for Stokes flows. *J. Fluid Mech.* **1975**, *67*, 787–815. [CrossRef]
19. Tang, P.; Greenwood, J.; Raper, J.A. A model to describe the settling behavior of fractal aggregates. *J. Colloid Interface Sci.* **2002**, *247*, 210–219. [CrossRef]
20. Veerapaneni, S.; Wiesner, M.R. Hydrodynamics of fractal aggregates with radially varying permeability. *J. Colloid Interface Sci.* **1996**, *177*, 45–57. [CrossRef]
21. Li, D.H.; Ganczarczyk, J. Fractal geometry of particle aggregates generated in water and wastewater treatment processes. *Environ. Sci. Technol.* **1989**, *23*, 1385–1389. [CrossRef]
22. Johnson, C.P.; Li, X.; Logan, B.E. Settling velocities of fractal aggregates. *Environ. Sci. Technol.* **1996**, *30*, 1911–1918. [CrossRef]
23. Dharmarajah, A.H. Effect of Particle Shape on Prediction of Velocity-Voidage Relationship in Fluidized Solid-Liquid Systems. Ph.D. Thesis, Iowa State University Capstones, Ames, IA, USA, 1982.
24. Johnstone, H.F.; Pigford, R.L.; Chapin, J.H. *Heat Transfer to Clouds of Falling Particles*; Technical Report; University of Illinois at Urbana Champaign, College of Engineering: Urbana, IL, USA, 1941.
25. Heywood, H. Uniform and non-uniform motion of particles in fluids. In Proceedings of the Symposium on Interactions between Fluids and Particles, London, UK, 20–22 June 1962; pp. 1–8.
26. Malaika, J. Effect of Shape of Particles on Their Settling Velocity. Ph.D. Thesis, Iowa State University, Ames, IA, USA, 1949.
27. Pettyjohn, E. Effect of particle shape on free settling rates of isometric particles. *Chem. Eng. Prog.* **1948**, *44*, 157–172.
28. Wadell, H. The coefficient of resistance as a function of Reynolds number for solids of various shapes. *J. Frankl. Inst.* **1934**, *217*, 459–490. [CrossRef]
29. Zenz, F.A.; Othmer, D.F. *Fluidization and Fluid-Particle Systems*, 1st ed.; Reinhold Chemical Engineering Series: New York, NY, USA, 1960.
30. Hartman, M.; Trnka, O.; Svoboda, K. Free settling of nonspherical particles. *Ind. Eng. Chem. Res.* **1994**, *33*, 1979–1983. [CrossRef]
31. Silva, R.; Garcia, F.A.; Faia, P.M.; Rasteiro, M.G. Settling suspensions flow modelling: A review. *KONA Powder Part. J.* **2015**, *32*, 2015009. [CrossRef]
32. Mendez, Y. A Flow Model for the Settling Velocities of non Spherical Particles in Creeping Motion, Part II. *J. Appl. Fluid Mech.* **2012**, *5* , 123–130.
33. Zbik, M.; Smart, R.S.C. Nanomorphology of kaolinites: Comparative SEM and AFM studies. *Clays Clay Miner.* **1998**, *46*, 153–160. [CrossRef]
34. Pruett, R.J.; Webb, H.L. Sampling and analysis of KGa-1 B well-crystallized kaolin source clay. *Clays Clay Miner.* **1993**, *41*, 514–519. [CrossRef]
35. Zegznda, A.P. Settlement of sand gravel particles in still water. *Izv. NIIG* **1934**, *12*. (In Russian)
36. Arkangel'skii, B.V. Experimental Study of Accuracy of Hydraulic Coarseness scale of Particles. *Izv. NIIG* **1935**, *15*. (In Russian)
37. Sarkisyan, A.A. Deposition of sediment in a turbulent stream. *Izd. AN SSSR* **1958**. (In Russian)
38. Cheng, N. Simplified settling velocity formula for sediment particle. *J. Hydraul. Eng.* **1997**, *123*, 149–152. [CrossRef]
39. Wang, C.; Pan, S.P.; Peng, G.S.; Tsai, J.H. A comparison study on the measurement of nanoparticles. In Proceedings of the Recent Developments in Traceable Dimensional Measurements III, San Diego, CA, USA, 31 July–1 August 2005; International Society for Optics and Photonics: Bellingham, WA, USA, 2005; Volume 5879, p. 587910.
40. Mucha, P.J.; Tee, S.Y.; Weitz, D.A.; Shraiman, B.I.; Brenner, M.P. A model for velocity fluctuations in sedimentation. *J. Fluid Mech.* **2004**, *501*, 71–104. [CrossRef]
41. Chakraborti, R.K.; Kaur, J. Noninvasive Measurement of Particle-Settling Velocity and Comparison with Stokes' Law. *J. Environ. Eng.* **2013**, *140*, 04013008. [CrossRef]
42. Raudkivi, A.J. *Loose Boundary Hydraulics*; CRC Press: Boca Raton, FL, USA, 1998.
43. Jansen, J.W.; De Kruif, C.G.; Vrij, A. Attractions in sterically stabilized silica dispersions: II. Experiments on phase separation induced by temperature variation. *J. Colloid Interface Sci.* **1986**, *114*, 481–491. [CrossRef]

44. Davis, K.E.; Russel, W.B.; Glantschnig, W. Settling suspensions of colloidal silica: Observations and X-ray measurements. *J. Chem. Soc. Faraday Trans.* **1991**, *87*, 411–424. [CrossRef]
45. Mendez, Y. A Flow Model for the Settling Velocities of non Spherical Particles in Creeping Motion. *J. Appl. Fluid Mech.* **2011**, *4*, 65–75.
46. Mendez, Y. A Proposed Solution for the Settling Velocity of Coplanar Aggregates of Identical Spheres in Creeping Motion. *J. Appl. Fluid Mech.* **2015**, *8*, 399–407. [CrossRef]
47. Lu, N.; Ristow, G.H.; Likos, W.J. The accuracy of hydrometer analysis for fine-grained clay particles. *Geotech. Test. J.* **2000**, *23*, 487–495.